Surface Ligand Effects on Metal-Affinity Coordination to Quantum Dots: Implications for Nanoprobe Self-Assembly

Allison M. Dennis, David Sotto, Bing C. Mei, Igor L. Medintz, Hedi Mattoussi, and Gang Bao

Supplementary Information

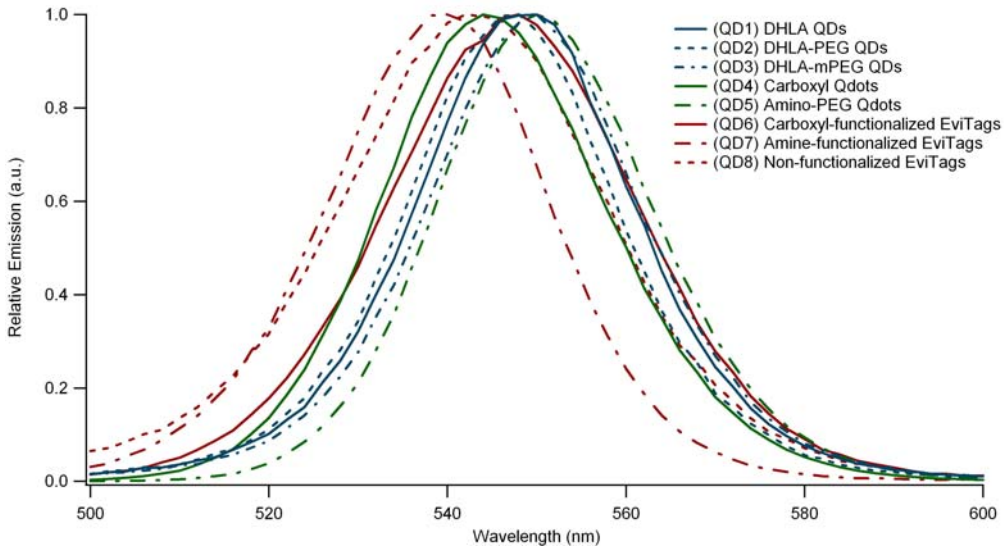

Figure S1: Emission spectra of 8 QD varieties excited at 400 nm.

Calculating the Donor-Acceptor Distance (*R*)

Using the FRET efficiencies determined for each QD:FP ratio and the Förster distance (R_0) calculated for each FRET pair, the distance between the donor and acceptor was estimated using an equation that takes into account the binding of multiple acceptors to each donor QD. The equation for the FRET efficiency as a function of *n*, the number of acceptors attached to the donor, is (*1, 2*)

$$E(n) = \frac{nR_0^6}{nR_0^6 + R^6}$$

For any given ratio of donors to acceptors (or average number of acceptors per donor), *n*, the actual number of acceptors attached to the donor, *k*, is described by the Poisson's Distribution (*3*):

$$p(k,n) = \frac{n^k e^{-n}}{k!}$$

For $k < 5$, the efficiency of the FRET interaction can be more accurately calculated for each donor-acceptor ratio using a weighted distribution of efficiencies, taking into account the effect of the Poisson distribution (*4, 5*).

$$E(n) = \sum_k p(k,n)E(k) = \sum_{k=1}^{\infty} \frac{n^k e^{-n}}{k!} \frac{kR_0^6}{(kR_0^6 + R^6)}$$

From this equation we can solve for *R* for each value of *n* for each pair. We used Mathematica (v6, Wolfram Research, Champaign, IL) for this purpose.

The calculated donor-acceptor distances for the four conditions it was the most relevant are listed in Table S1. While the trends are the same whether the Poisson's distribution was used or not, significant differences in the resulting donor-acceptor distances were apparent in cases where significant FRET efficiencies were observed at low acceptor to donor ratios. This discrepancy, which is the most dramatic for the carboxyl-functionalized EviTags (QD6), is due to the underestimation of the donor-acceptor distance that occurs at low acceptor to donor ratios when the Poisson's distribution is not taken into account. Errors of up to 40% have been described as theoretically possible at 1:1 acceptor to donor ratios (*3*).

Assessing QD Stability

The stability of the QD photoluminescence (PL) over time was assessed in the two buffers used in this study: 10 mM tetraborate, 154 mM NaCl, pH 9.5 and 10 mM tetraborate, 1 M NaCl, pH 9.5. Quantum dots were loaded into the same flat-bottomed, non-binding, 384-well plates used for the FRET assays and their fluorescence emission was measured as soon as feasible and every 10 minutes thereafter for a total of 500 minutes in a Tecan Safire^2 with 400 nm excitation. Significant fluctuations in the QD PL were seen in all of the samples in the first several readings.

Table S1: Results of *R* value calculations.

	Amine-functionalized EviTags[a]		Carboxyl-functionalized EviTags		DHLA			Carboxyl Qdots with Ni2+	
FP:QD[b]	+[c]	-[d]	+	-	+	-	FP:QD	+	-
0.25	69.6	64.5	52.4	35.5	59.8	57.9	0.167	82.4	80.0
0.5	66.0	59.6	52.3	39.6	57.2	55.0	0.334	99.7	98.8
0.75	65.5	59.4	52.3	42.1	57.3	55.2	0.5	126.7	126.4
1	65.0	59.3	52.4	43.9	60.1	58.4	0.668	95.0	93.9
1.5	66.5	62.2	53.2	47.3	56.8	54.9	1	90.5	89.2
2	68.4	65.0	53.8	49.3	57.8	56.1	1.336	86.6	84.9
3	70.6	68.1	55.2	52.2	58.8	57.4	3	91.1	90.0
4	72.2	70.3	56.9	54.7	59.2	58.0	4	92.9	91.9
6	75.5	74.1	59.3	57.8	62.0	61.2	6	94.2	93.3
8	77.7	76.6	62.3	61.2	64.3	63.6	8	95.1	94.4
12	82.1	80.8	65.7	64.3	69.8	69.0	12	97.3	96.2
Range	65.0-82.1	59.3-80.8	52.3-65.7	35.5-64.3	56.8-69.8	54.9-69.0		82.4-126.7	80.0-126.4
Mean	70.8	67.35	56.0	49.8	60.3	58.8		95.6	94.5
Median	69.6	65.0	53.8	49.3	59.2	57.9		94.2	93.3

[a] All distance values reported are in angstroms (Å).
[b] The ratio of acceptor to donor molecules.
[c] Calculation of the donor-acceptor distance *with* application of the Poisson's distribution.
[d] Calculation of the donor-acceptor distance *without* application of the Poisson's distribution.

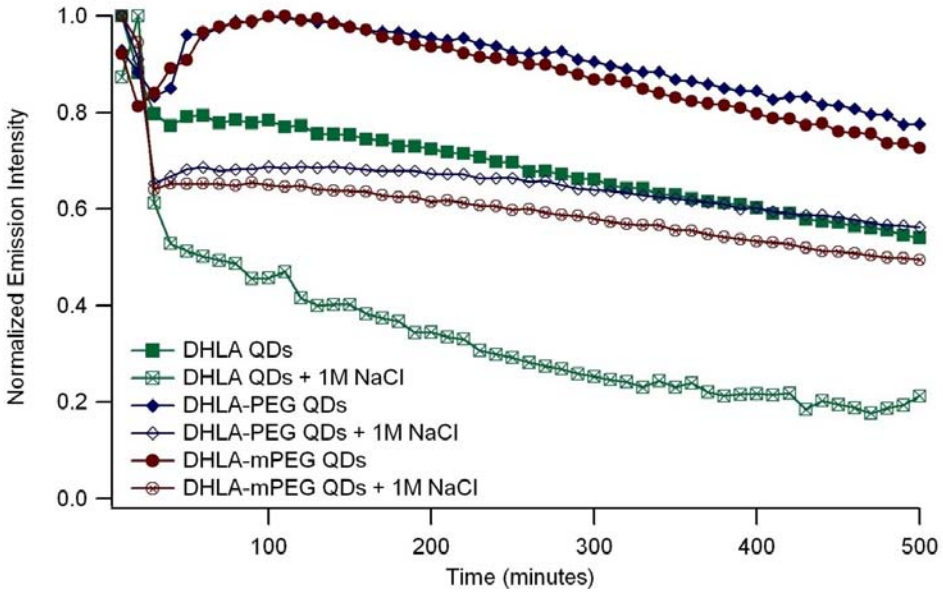

Figure S2: Stability plot of DHLA-coated QDs (QD1-QD3).

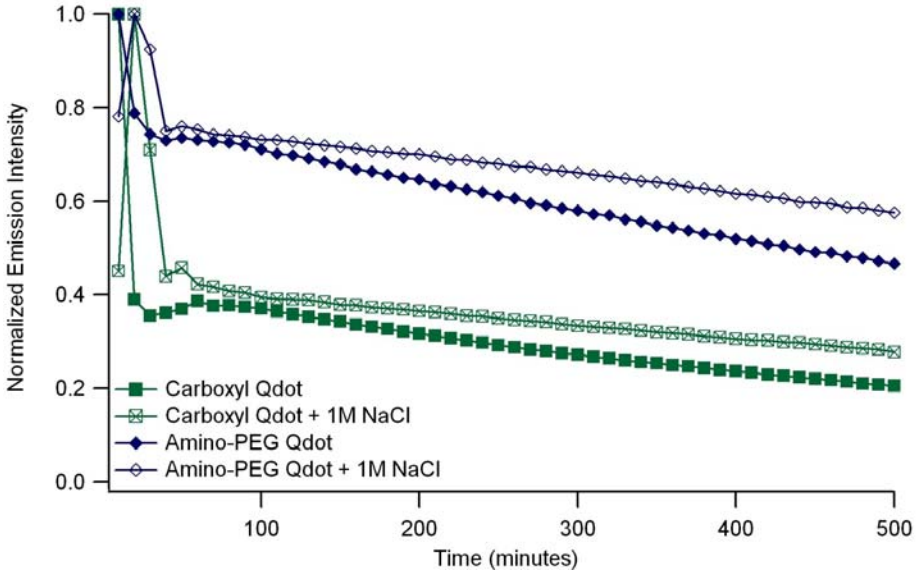

Figure S3: Stability plot of Qdots from Invitrogen (QD4-QD5).

All of the DHLA-coated QDs (QD1-QD3) exhibited an approximately 20% decrease in PL in the first several readings after being dispersed in 10 mM tetraborate buffered saline, pH 9.5 (Figure S2). While the PEGylated QDs recovered their initial PL intensity (QD2-QD3), the QDs coated only with DHLA (QD1) did not recover, but did reach a stasis where the PL was much better maintained from one measurement to the next. All three of the QD types showed slow, but steady, declines in the PL intensity

with time. Under high salt conditions, the PEGylated QDs did not show the same PL recovery seen in saline, but were stable enough to exhibit only a very gradual decrease in PL intensity with time once equilibrium was reached. The QDs coated with only DHLA, in contrast, were not stable in the high salt conditions and demonstrated a dramatic decrease in PL over time. This is likely due to the flocculation of the QDs, since the high salt conditions mitigated the effect of electrostatic stabilization usually conferred by the high density of carboxyl groups on the QD surface.

The PL of Qdots from Invitrogen also showed instability immediately following dilution into the buffers (Figure S3). Although the carboxyl Qdots (QD4) showed a much larger decrease in PL in the first few measurements than the amino-PEG Qdots (QD5), there were not significant differences for each Qdot between the saline and high salt conditions. This was the case for the carboxyl Qdots even though the poly(acrylic acid) used to confer water solubility to the QD is highly negatively charged. In contrast to the DHLA QD, the thick polymer coating of the carboxyl Qdot must stabilize the nanoparticle sterically as well as electrostatically.

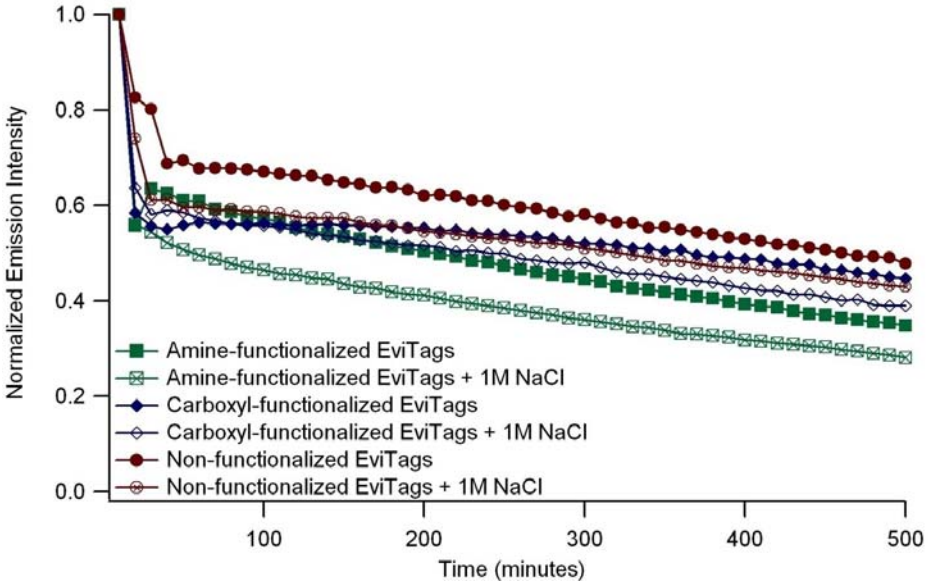

Figure S4: Stability plot of T2-MP EviTags from Evident Technologies (QD6-QD8).

All of the EviTags (QD6-QD8) dropped 30 – 40% of their PL in the first few measurements before achieving a certain level of PL stability (Figure S4). No significant differences were seen based on coating functionality or buffer conditions.

The PLs were erratic for the first 10% of the stability measurements by time, but thereafter the data

points could be fit to a line. The value of that slope was graphed in Figure S5 to summarize the differences in the rate of PL change for all of the QDs and buffer conditions.

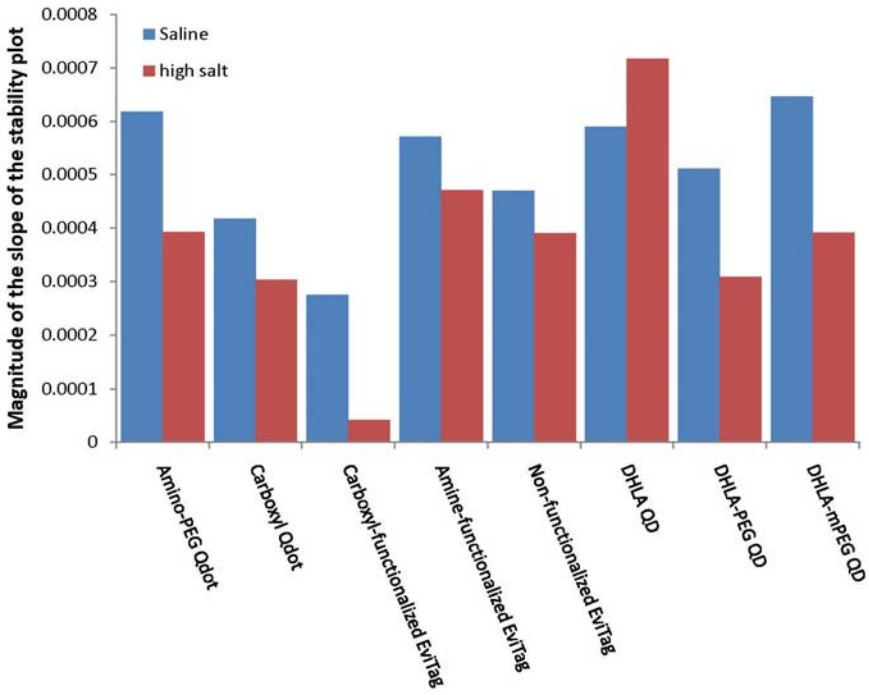

Figure S5: Magnitude of the slopes of the stability plots.

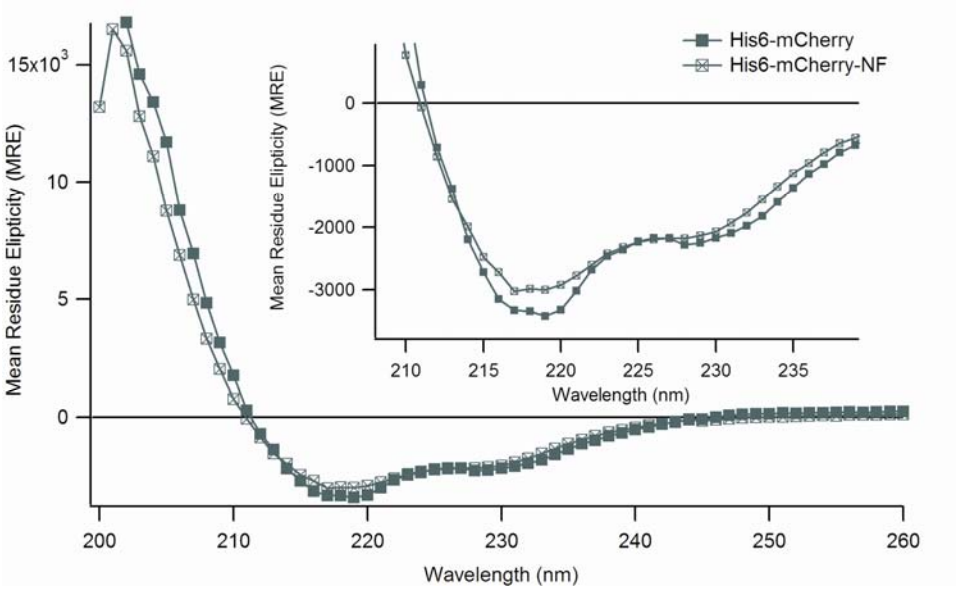

Figure S6: CD spectra of His6-mCherry and His6-mCherry-NF.

The QD PL instability could be a result of several processes. Some aggregation of the QD may be taking place as well as binding to the walls of the micro-well plate. In addition, incomplete mixing of small volumes could complicate the measurements. Based on our observation of the PL instability when diluted into a fresh buffer, all of the QDs were diluted in buffer early in the experimental preparation and allowed to equilibrate in a microcentrifuge tube before being added to the protein solutions that were already pipetted into the micro-well plate. As described in the Materials and Methods, the QDs were then incubated with the protein for at least fifteen minutes before the measurement to allow for self-assembly of the nanoprobe.

Characterization of His6-mCherry-NF

A non-fluorescent analogue to the His6-mCherry was developed to see what effect binding of the his-tagged protein had on the QDs, apart from the observed FRET signal. This protein was expressed and purified in a manner identical to the His6-mCherry. Further characterization was necessary, however, to show that the protein structure was maintained despite the mutations and to assess the spectral properties of the protein. Circular dichroism (CD) was used to show that the mutated mCherry still maintained the characteristic beta sheets present in the barrel structure of GFP-like proteins (*6, 7*). A Jasco J-815 CD Spectrometer (Jasco, Inc., Easton, MD) was used measure 20 µM (56 µg/mL) solutions of both His6-mCherry and His6-mCherry-NF. The two CD spectra overlap nicely (Figure S6), including the double hump seen between 215 and 235 nm, which is characteristic of beta sheets (Figure S6, inset). Absorbance and emission measurements (with excitation at 560 nm) of 10 µM (28 µg/mL) solutions of the two proteins were made on a Tecan Safire^2 multiplate reader. His6-mCherry-NF showed no capacity for either absorbance or emission in the visible wavelength range (Figure S6). The emission of His6-

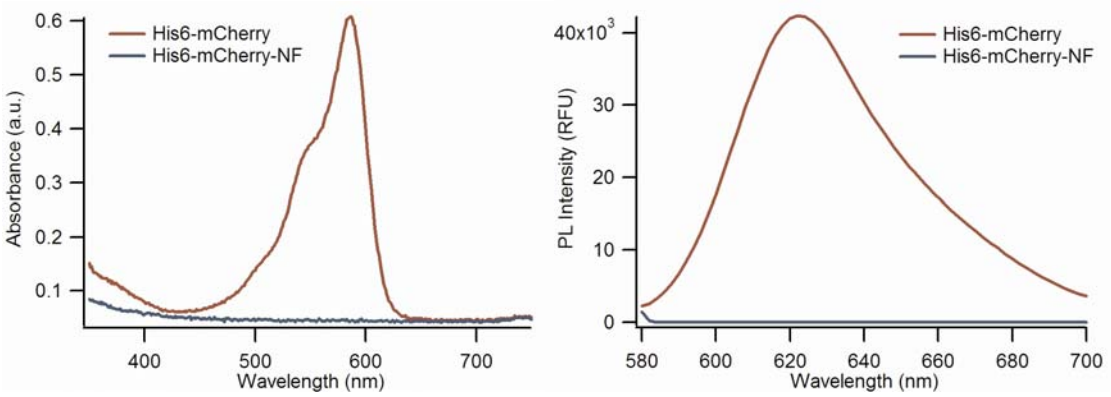

Figure S7: Absorbance (left) and emission (right) spectra of His6-mCherry and His6-mCherry-NF.

mCherry-NF remained flat even with greatly increased detector sensitivity (data not shown). The absorbance and emission spectra of His6-mCherry and His6-mCherry-NF are shown in Figure S7.

Effect of His-tag binding on QD Photoluminescence

Each of the QDs was incubated with varying amounts of two different his-tagged proteins to see if the his-tag binding itself had any effect on the QD PL in this assay format. Maltose binding proteins (MBP) with a his5 sequence were used as has been previously described (*8*). His6-mCherry-NF was used as well

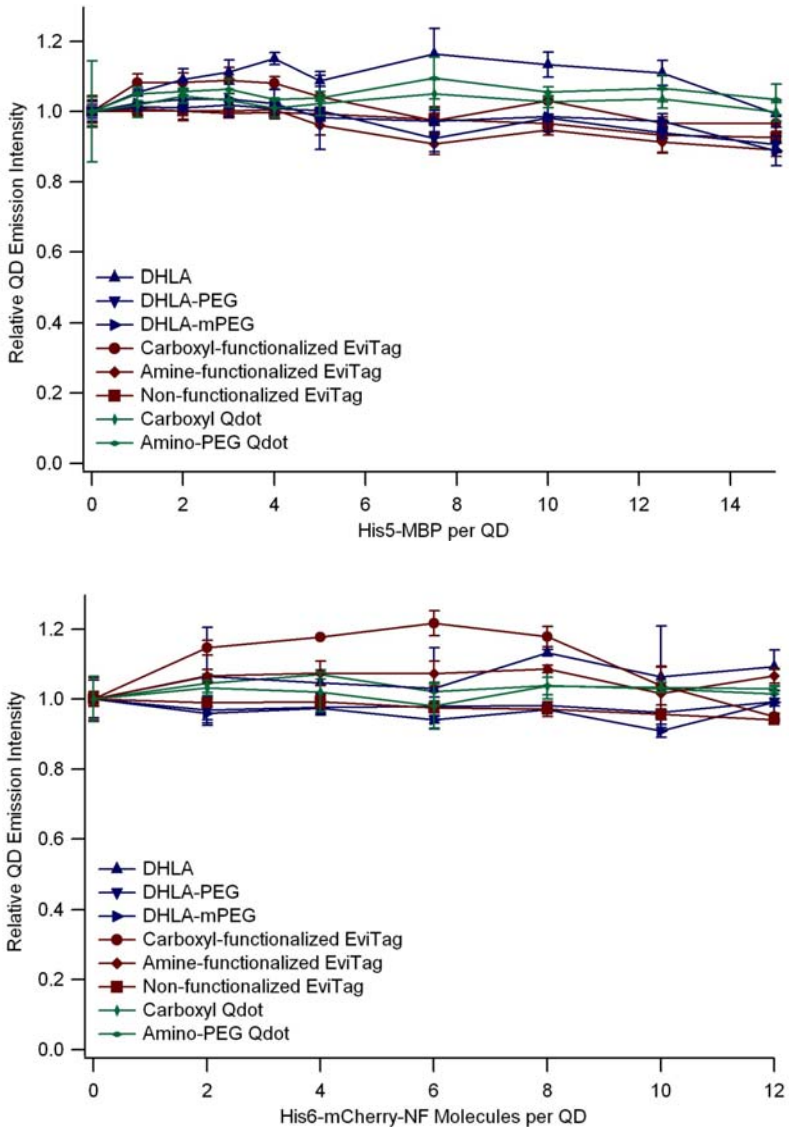

Figure S8: Relative emission of QDs incubated with varying concentrations of either His5-MBP (top) or His6-mCherry-NF (bottom).

to provide an alternative that has the same protein structure as the His6-mCherry used in the other experiments. The same experimental protocols and data analysis techniques were used for these assays as was described in the text for the FRET assays using the fluorescent proteins.

The DHLA-coated QDs showed the largest PL increase in response to binding from the His5-MBP with an almost 20% increase in the QD emission (Figure S8, top). The carboxyl-functionalized EviTags showed a similar increase, but in the presence of the His6-mCherry-NF (Figure S8, bottom). This could be an indication that each of these QDs has some exposed surface defects that are filled by the binding of the polyhistidine peptide. In both cases, however, the effect was not reliably dose-dependent.

Effect of Modified FRET Assay Protocol on Quenching Profile

In order to account for the small increase seen in the PL of some QDs upon binding of a non-fluorescent his-tagged protein, a modified FRET assay was performed in which the total number of proteins in the solution was maintained, but the ratio of fluorescent to non-fluorescent proteins was varied. DHLA-coated QDs were incubated with a total of 12 proteins per QD: the total number of His6-mCherry was increased with corresponding decreases in either His6-mCherry-NF or His5-MBP. There was not a dramatic difference between the experiments using His6-mCherry-NF or using His5-MBP, but the shape of those two quenching curves was distinct from that of the DHLA-coated QDs incubated with His6-mCherry in the absence of any filler proteins (Figure S9, top). It is possible that the non-fluorescent proteins proved to be competition for binding on the QD surface, thereby mitigating the positive effect that could have been seen by enhancing the QD PL. The carboxyl-functionalized EviTags were likewise incubated with a mix of His6-mCherry-NF and His6-mCherry, but in this case the total number of proteins in solution was limited to six per QD. The carboxyl-functionalized EviTags exhibited the same quenching profile with or without the His6-mCherry-NF filler proteins present (Figure S9, bottom), but at each FP:QD ratio there was slightly less quenching in the presence of the non-fluorescent protein. Here, again, a competition for the binding sites on the ZnS shell layer of the QD may have contributed to that difference.

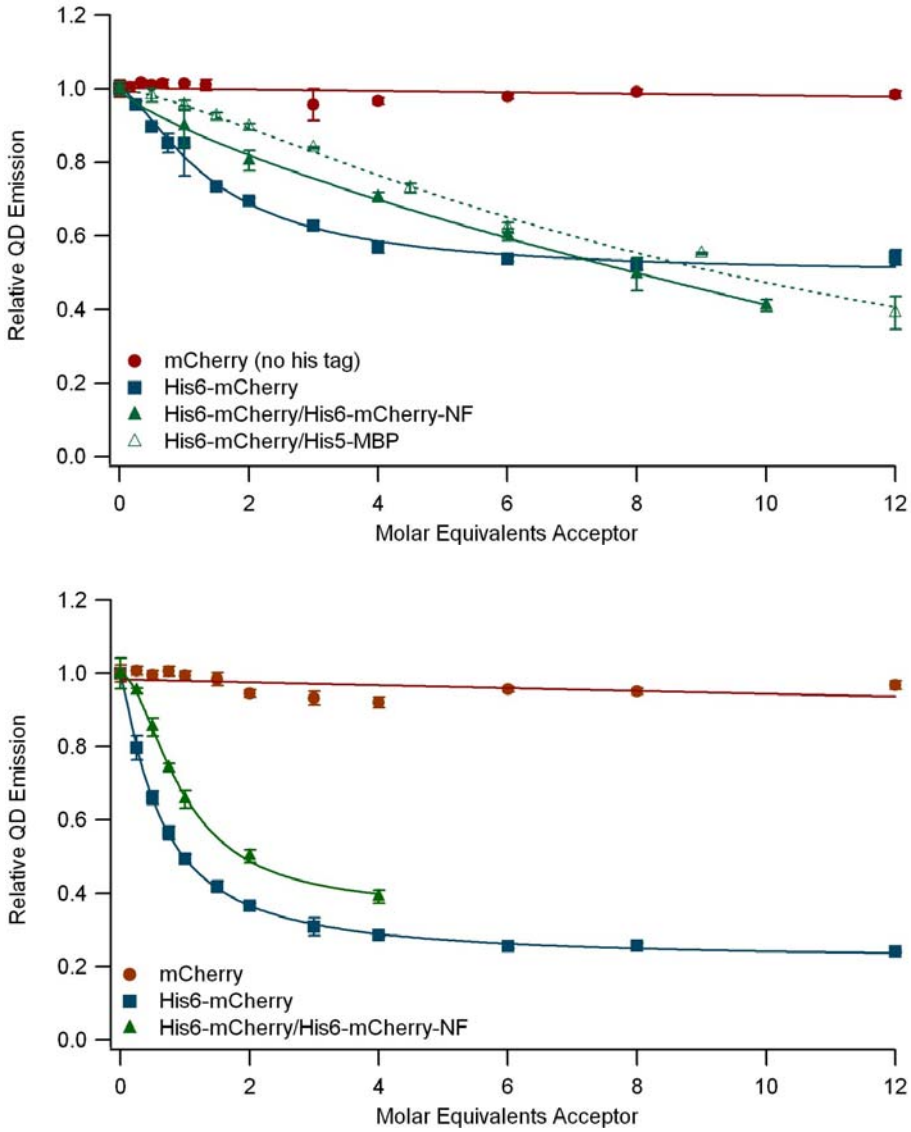

Figure S9: Effect of using a mixture of fluorescence and non-fluorescent proteins in FRET assay on DHLA-coated (top) and carboxyl-functionalized EviTags (bottom).

References

(1) Medintz, I. L., Clapp, A. R., Mattoussi, H., Goldman, E. R., Fisher, B., and Mauro, J. M. (2003) Self-assembled nanoscale biosensors based on quantum dot FRET donors. *Nat Mater 2*, 630-8.

(2) Lakowicz, J. R. (2006) *Principles of fluorescence spectroscopy*, 3rd ed., Springer, New York.

(3) Pons, T., Medintz, I. L., Wang, X., English, D. S., and Mattoussi, H. (2006) Solution-phase single quantum dot fluorescence resonance energy transfer. *J Am Chem Soc 128*, 15324-31.

(4) Medintz, I. L., Berti, L., Pons, T., Grimes, A. F., English, D. S., Alessandrini, A., Facci, P., and Mattoussi, H. (2007) A reactive peptidic linker for self-assembling hybrid quantum dot-DNA bioconjugates. *Nano Lett 7*, 1741-8.

(5) Medintz, I. L., Clapp, A. R., Brunel, F. M., Tiefenbrunn, T., Uyeda, H. T., Chang, E. L., Deschamps, J. R., Dawson, P. E., and Mattoussi, H. (2006) Proteolytic activity monitored by fluorescence resonance energy transfer through quantum-dot-peptide conjugates. *Nat Mater 5*, 581-9.

(6) Sreerama, N., Venyaminov, S. Y., and Woody, R. W. (1999) Estimation of the number of alpha-helical and beta-strand segments in proteins using circular dichroism spectroscopy. *Protein Sci 8*, 370-80.

(7) Vrzheshch, P. V., Akovbian, N. A., Varfolomeyev, S. D., and Verkhusha, V. V. (2000) Denaturation and partial renaturation of a tightly tetramerized DsRed protein under mildly acidic conditions. *FEBS Lett 487*, 203-8.

(8) Clapp, A. R., Medintz, I. L., Mauro, J. M., Fisher, B. R., Bawendi, M. G., and Mattoussi, H. (2004) Fluorescence resonance energy transfer between quantum dot donors and dye-labeled protein acceptors. *Journal of the American Chemical Society 126*, 301-310.